Corners, Cusps, and Pearls in Running Drops

T. Podgorski,* J.-M. Flesselles,† and L. Limat

Physique et Mécanique des Milieux Hétérogènes, UMR 7636 CNRS-ESPCI, 10 rue Vauquelin, 75231 Paris Cedex 05, France

(Received 6 February 2001; published 27 June 2001)

Small drops sliding down a partially wetting substrate bifurcate between different shapes depending on their capillary number Ca. At low Ca, they are delimited by a rounded, smooth contact line. At intermediate values they develop a corner at the trailing edge, the angle of which evolves from flat to 60° with increasing velocity. Further up, they exhibit a cusped tail that emits smaller drops ("pearls"). These bifurcations may be qualitatively and quantitatively recovered by considering the dynamic contact angle along the contact line.

DOI: 10.1103/PhysRevLett.87.036102 PACS numbers: 68.03.Cd, 47.15.Gf, 47.20.Dr, 68.08.Bc

The formation and detachment of drops from a nozzle is a well known phenomenon. Provided that drops are sufficiently small, they are perfectly spherical except at breakup where a singularity occurs. A detailed description of this singularity has only recently been achieved [1]. Similar cusplike shapes are found when a bubble rises through a polymer or micellar solution [2,3], though in this particular case the viscoelastic nature of the fluid is a crucial feature of the problem.

In comparison, drops running down an inclined surface have received less attention. However, it is a common experience that drops running on a window pane can exhibit complex and fascinating behaviors, involving singularities, coalescence, and breakup. Indeed wetting and dewetting phenomena arising from the interaction with the solid substrate lead to increased complexity.

Early experimental studies and theories involving drops sliding under the action of gravity over an inclined surface were aimed at determining the conditions for which droplets remain pinned on an inclined surface [4,5]. The shape of static or quasistatic drops and the yield conditions for displacement under the action of gravity or external shear flows were considered in asymptotic theories [6,7] and recent numerical studies [8]. In all these works, the drops are assumed to be close to equilibrium, and contact angles close to their static values.

Drops moving at higher velocities were studied in the case of contact angles close to 180°, i.e., when the solid is almost fully nonwettable. In this case, drops have a roughly spherical shape and roll down the slope instead of sliding or flowing [9,10]. However, drops running down a plane at significant velocities and with usual values of the contact angles have not been accurately described yet despite the simplicity, at least in principle, of the experiment.

We report here well controlled experiments showing that drops may exhibit various shapes and remarkable spatiotemporal patterns. In particular, above a critical capillary number, drops depart from their classical rounded shape and exhibit a corner at the trailing edge. This corner becomes sharper as the velocity is further increased, up to 60° where a second threshold is reached above which smaller droplets are released behind the main drop. Several bifurcations involving frequency divisions in the droplet release occur when increasing the capillary number. We show that the transitions between different shapes depend only on the physical properties of the fluid/substrate couple and we relate them to flow transitions occurring in coating devices.

The main part of the experimental setup is a 20×20 cm glass plate which can rotate about a horizontal axis to vary its inclination between 0° and 90°. The surface has been coated with a fluoro-polymer (FC725 from 3M) in order to have a low air-substrate surface tension (about 13 mN/m). In these conditions, poly-dimethyl-siloxane (PDMS) also known as silicon oil (Rhodorsil brand), wets partially the surface with a static advancing contact angle of about 50° and a static receding contact angle of about 40°. Such experimental conditions have several advantages: high reproducibility and good control of wetting characteristics, availability of silicone oil with a variety of viscosities. Three types of silicon oil were used (main characteristics summarized in Table I). Some measurements were also made with water on a polyacrylate substrate to extend the range of explored parameters. Drops of controlled size are emitted at a constant rate by a pipette fixed above the upper part of the inclined plate. Typical volume of emitted drops range from 2 to 20 mm^3 (drop radius of 0.8 to 1.7 mm). After deposition on the surface, the drops flow down the plate and reach within a few millimeters a stationary state: constant velocity, and if applicable constant shape.

Drops are transparent, hence hard to observe without appropriate lighting. With a mask placed behind the glass plate, we set a strong illumination gradient perpendicular to the direction of flow. Drops act as focusing lenses and appear on the inhomogeneous background, giving a striking three-dimensional impression (Fig. 1). The motion was recorded via a CCD camera and frame grabber at a rate of one to five frames per second and 1/500 s exposure time. The frames were then de-interlaced.

Drops are continuously produced at a frequency of about 1 Hz and we measure their velocity U and record their shape for various inclinations of the plate α. Since for a

TABLE I. Main characteristics of liquid-substrate systems used in the experiments. 47V*xx* denotes silicon oil type.

Fluid	Substrate	η (cP)[a]	γ (mN/m)	θ_r (°)	Y_w (nm)	A (comp.)	A (exp.)
47V2	FC725	2.33	18.7	35 ± 2	10	9.7×10^{-3}	1.1×10^{-2}
47V10	FC725	9.15	20.5	42 ± 2	20	1.0×10^{-2}	1.1×10^{-2}
47V50	FC725	50.2	20.7	43 ± 2	60	1.1×10^{-2}	1.2×10^{-2}
Water[b]	Polyacrylate	0.891	72.0	30 ± 5	1	8.0×10^{-3}	4.4×10^{-3}

[a]Recorded at 25 °C.
[b]Ultrapurified (deionized).

given drop volume the velocity U is an increasing function of α, we actually control U by varying α. At low velocities, small drops (i.e., with radii of order or smaller than the capillary length) have an essentially regular contour and appear as circles or ovals [Figs. 1(a) and 1(b)]. Upon increasing velocity, drops deform and the contact line eventually develops a corner along the trailing edge suggesting a curvature singularity at the tip [Figs. 1(c)–1(e)]. As the velocity is increased, the corner becomes sharper up to an angle close to 60° where it jumps to a cusp (0°) which releases small droplets [Fig. 1(f)]. When the velocity is further increased, a tail develops which is unstable via a Rayleigh-like instability [11,12]. It breaks into regular equally spaced smaller drops which are too light to flow and remain pinned on the surface [Fig. 1(g)]. The final pattern appears as pearling drops running along a line of static smaller droplets left by the previous drop. These droplets are absorbed from the front and recreated in the back, which ensures mass conservation and a stationary regime. In the first stages of this regime, droplets are very small compared to the main drop, and their absorption by the next drop is not a sufficient perturbation to induce a measurable fluctuation of its velocity or a correlation between absorption and emission of droplets. For higher velocities, a cascade of bifurcations involving frequency divisions takes place, and the emission of droplets exhibits a rich variety of dynamical periodic patterns [Fig. 1(h)]. Emitted droplets eventually become large enough to start running on the substrate, giving rise to even more complex behavior. The absorption of droplets becomes a significant perturbation and couples the dynamics of successive drops.

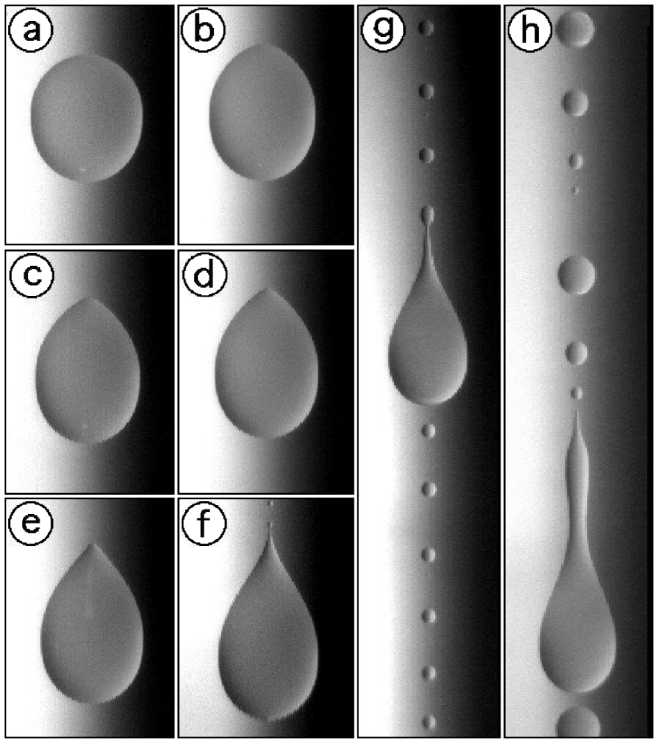

FIG. 1. Different shapes of a drop running down a plate when increasing velocity (by increasing inclination). Drops flow downwards. (a),(b) Rounded drops at low speed, (c)–(e) corner drops becoming sharper as velocity increases, (e) corner angle of 60° just before transition to pearling drops, (f) first stage of the pearling drop regime, (g) pearling drop releasing droplets of constant size at a constant rate, and (h) pearling drop releasing periodic series of droplets at higher velocity.

Intuitively, the velocity U of a drop of volume V should be mainly governed by the in-plane component of its weight $\rho g V \sin\alpha$, where ρ is the fluid density and g is the acceleration of gravity, and a typical viscous drag force of order $\eta V^{1/3} U$ where η is the viscosity. Another force of capillary origin is also balancing the weight because of the nonuniformity of the contact angle along the perimeter of the drops, i.e., because of the contact angle hysteresis. This force scales as $\gamma V^{1/3} \Delta_\theta$, where γ is the surface tension and Δ_θ is a perimeter-averaged projection factor of surface tension. Without going through a detailed calculation which would involve the exact shape of the drop and the associated three-dimensional flow field, this simple force balance implies that the following scaling law should be satisfied by the capillary number $Ca = \eta U/\gamma$ and the Bond number $Bo = V^{2/3} \rho g/\gamma$:

$$Ca \sim Bo \sin\alpha - \Delta_\theta . \qquad (1)$$

$Bo \sin\alpha$ and Ca are appropriate dimensionless scaling parameters for this problem, as can be seen in Fig. 2 where all data for a given fluid/substrate system fall on the same curve.

Below a minimum value $Bo_m = \Delta_\theta$ of $Bo \sin\alpha$, a drop remains pinned on the surface. Derivation of Bo_m can be found in Furmidge [5] and Dussan [6]. Above this threshold, Ca increases nearly linearly with $Bo \sin\alpha$ as expected from dimensional analysis [Eq. (1)], even when drops move at significant speed. However, the slope is

noticeably higher in the pearling regime. This can be qualitatively interpreted as an effect of "drag reduction" associated with the release of droplets at the trailing edge and acceleration associated with absorption of droplets left behind the previous drop at the front. Finally, Fig. 2 shows that the transitions between the different regimes are independent of the drop size and depend only on a critical capillary number Ca.

These transitions can be related to observations of dynamic wetting failure occurring in coating devices [13,14]. In that context, the contact line comes to an oblique position with respect to the direction of motion when the speed becomes large enough. For instance, when a plate is withdrawn from a pool, the wetting line remains static and horizontal at low speeds and takes a saw tooth shape when the speed is greater than a "maximum speed of dewetting." It eventually releases small drops at the tip, which are entrained by the moving substrate [14] at higher withdrawal speeds. This is quite similar to what we observe at the trailing edge of our liquid drops.

It is experimentally known that the dynamic contact angle depends on the velocity (or Ca) of the wetting line [13]. Although no extended theory has been agreed upon, the experimental dynamic contact angle θ_d roughly follows a hydrodynamic theory [15,16] for many liquids. Following Blake and Ruschak [14], we further assume that the contact angle depends only on the velocity component normal to the contact line. In the general case, the relation linking θ_d to Ca involves complicated integral functions of the contact angle and viscosity ratio as shown by Cox [16]. However, for contact angles up to $3\pi/4$, it can be reduced to the simple expression with less than 3% error:

$$\theta_d^3 = \theta_s^3 + 9\left(\ln\frac{Y}{Y_w}\right)\mathbf{U}\cdot\mathbf{n}\,, \tag{2}$$

where θ_s is the static contact angle (θ_r for receding contact lines, θ_a for advancing), Y is a macroscopic length over which the contact angle is defined (about 1 mm), Y_w is a microscopic length under which macroscopic hydrodynamics fails (of order a few molecular sizes), $\mathbf{U}$ is the velocity of the fluid at the contact line, and $\mathbf{n}$ the external normal to the contact line (Fig. 3). Thus, when pulling a plate out of (into) a bath, the contact angle can reach 0° (180°) as the velocity is increased, eventually leading to liquid (air) entrainment. Blake and Ruschak interpret the obliquity of the contact line as a marginal state where $\theta_d = 0$ without fluid entrainment: $\mathbf{U}\cdot\mathbf{n}$ is below the entrainment threshold while U can be above. In our case, we assume that the orientation ϕ of the contact line adapts to keep $\mathbf{U}\cdot\mathbf{n} = Ca\sin\phi$ constant and such that $\theta_d \simeq 0°$, i.e., at the verge of liquid entrainment. Hence in the cornered drop regime,

$$Ca\sin\phi = A\theta_r^3\,, \tag{3}$$

where $A = (9\ln[Y/Y_w])^{-1}$ is a constant that characterizes the fluid only.

We measured the angle ϕ between the contact line and the direction of motion at the trailing edge in the cornered drop regime (Fig. 3). As can be seen in Fig. 4, experimental data for water and several silicon oils are compatible with Eq. (3). Note that physical properties vary significantly between different experiments. The experimental constant A obtained by fitting Eq. (3) agrees with roughly estimated values computed from $Y = 1$ mm and $Y_w \simeq 10$ molecular sizes for silicon oils (Table I). It is of the right order of magnitude for water, for which contact angle is known with a bad precision. Though A does not vary much between different fluids because the molecular size appears in a logarithm, the assumption that cornered drops or a sawtoothlike contact line occurs when θ_d is negligible

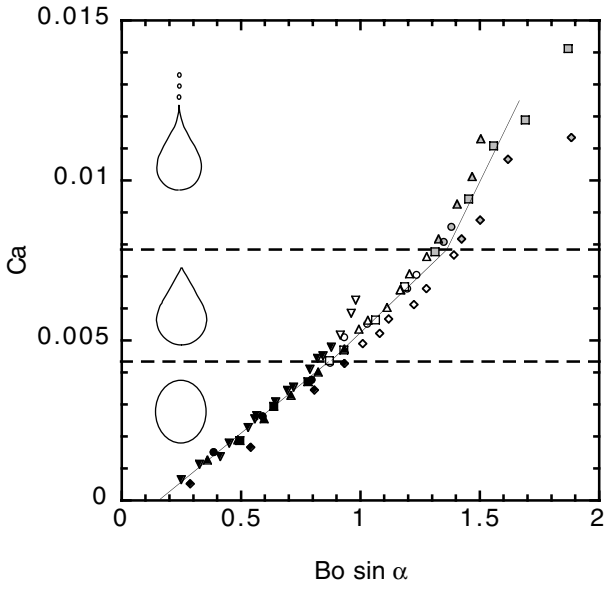

FIG. 2. Ca versus $Bo\sin\alpha$ number for 47V10 silicon oil. Drop volumes range from 3 to 18 mm^3 (▽: 3 mm^3; △: 5.5 mm^3; □: 8 mm^3 ; ∘: 11 mm^3; ◇: 18 mm^3). Horizontal dashed lines show the transitions between the different regimes (black: rounded, white: corner, and grey: pearling).

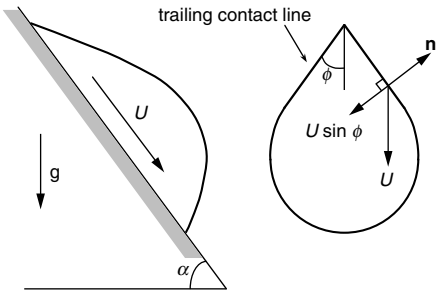

FIG. 3. Schematic of a drop running down a plate and notations. Left: side view of a drop running down a plate. Gravity is the driving force. U is the velocity of the drop (mean velocity of the fluid). Right: notations in the cornered drop regime.

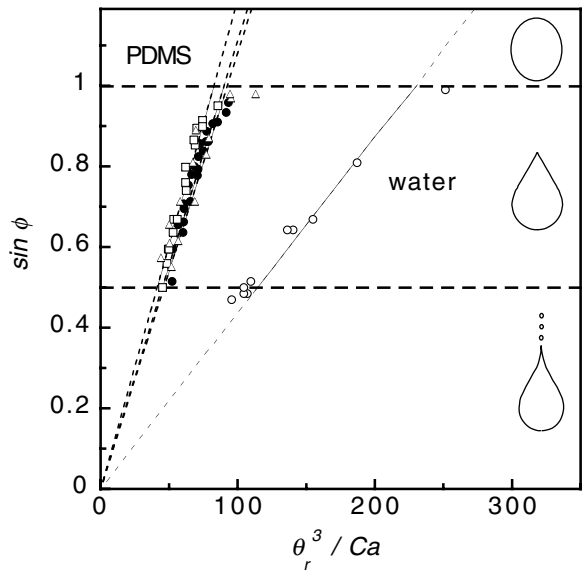

FIG. 4. Measured values of ϕ vs θ_r^3/Ca in the cornered drop regime for various liquid/substrate systems: (△) 47V2 oil/fluoropolymer, (•) 47V10 oil/fluoropolymer, (□) 47V50 oil/fluoropolymer, (∘) water/polyacrylate. Theoretical linear relation from Eq. (3) was fitted on the data by adjusting parameter A (see values in Table I). The horizontal dashed lines show the transitions to rounded drops at $\sin\phi = 1$ and to pearling drops at $\sin\phi = 1/2$.

is compatible with the experiment when using a simplified model of dynamic contact angle.

Expressions for the thresholds between different regimes can now be deduced from Eq. (3). At the rounded-corner transition, $\sin\phi = 1$ and the capillary number is

$$Ca_1 = A\theta_r^3 . \tag{4}$$

At the corner-pearling transition, we experimentally have $\sin\phi = 1/2$, hence the capillary number is

$$Ca_2 = 2A\theta_r^3 . \tag{5}$$

These critical capillary numbers, which can be measured on a macroscopic scale, depend only on the fluid-solid-gas interactions and microscopic properties of the fluid.

With well controlled experiments, we have shown that drops running down an inclined surface can exhibit various shapes (rounded, corners, and pearling). We identified the capillary number as the control parameter governing the transitions between different states. We related these transitions to the dynamic contact angle at the trailing edge of the drop and related this problem to air entrainment in coating applications.

The corner formation is linked to the existence of conical similarity solutions to the lubrication equations governing the flow near the tip of the drop. An interpretation for the occurrence of the transition from corner to pearling drops is the appearance of another static conical solution. We report this theoretical work in a forthcoming publication [17].

We thank M. Fermigier for fruitful suggestions and H. Stone and S. K. Wilson for valuable discussions on theoretical aspects of this work.

*Present address: Department of Mathematics, Penn State University, University Park, PA 16802.
†Present address: Saint Gobain Recherche, 93300 Aubervilliers, France.

[1] J. Eggers, Rev. Mod. Phys. **69**, 865 (1997).
[2] Y. Liu, T. Y. Liao, and D. D. Joseph, J. Fluid Mech. **304**, 321 (1995).
[3] A. Belmonte, Rheol. Acta **39**, 554 (2000).
[4] J. J. Bikerman, J. Colloid Sci. **5**, 349 (1950).
[5] C. G. L. Furmidge, J. Colloid Sci. **17**, 309 (1962).
[6] E. B. Dussan V and T. P. Chow, J. Fluid Mech. **137**, 1 (1983); E. B. Dussan V, *ibid.* **151**, 1 (1985).
[7] E. B. Dussan V, J. Fluid Mech. **174**, 381 (1987).
[8] P. Dimitrakopoulos and J. J. L. Higdon, J. Fluid Mech. **377**, 189 (1998); **395**, 181 (1999).
[9] L. Mahadevan and Y. Pomeau, Phys. Fluids **11**, 2449 (1999).
[10] D. Richard and D. Quéré, Europhys. Lett. **48**, 286 (1999).
[11] D. B. Bogy, Annu. Rev. Fluid Mech. **11**, 207 (1979).
[12] S. P. Lin and R. D. Reiz, Annu. Rev. Fluid Mech. **30**, 85 (1998).
[13] T. D. Blake and K. J. Ruschak, in *Liquid Film Coating,* edited by F. Kistler and P. Schweitzer (Chapman and Hall, London, 1997).
[14] T. D. Blake and K. J. Ruschak, Nature (London) **282**, 489 (1979).
[15] O. V. Voinov, Fluid Dyn. **11**, 714 (1976).
[16] R. G. Cox, J. Fluid Mech. **168**, 169 (1986).
[17] H. A. Stone, L. Limat, S. K. Wilson, J.-M. Flesselles, and T. Podgorski, C. R. Acad. Sci. Paris (to be published).